Catalysis Science & Technology

ROYAL SOCIETY OF CHEMISTRY

PAPER

View Article Online
View Journal

Cite this: DOI: 10.1039/d4cy00715h

Electrocatalytic reduction of nitrite to ammonium ion using Ni(II) complexes with redox-active di(imino)pyridine ligands†

Somayeh Norouzinyanlakvan, Jeffrey Ovens and Darrin Richeson *

Received 5th June 2024,
Accepted 25th July 2024

DOI: 10.1039/d4cy00715h

rsc.li/catalysis

Human disruption of the nitrogen cycle motivates the exploration into electrocatalytic reduction of nitrite. Homogeneous Ni(II) complexes with tridentate redox-active bis(imino)pyridine ligands demonstrated high effectiveness and selectivity for electrocatalytic reduction of nitrite to the ammonium ion and hydroxylamine in solutions buffered with 4-morpholinepropanesulfonic acid (MOPS). Controlled potential coulometry at −1.4 V *vs.* $Fc^{0/+}$ predominantly produced the ammonium ion with Faradaic efficiencies of ≥50%. Foot-of-the-wave analysis yielded calculated turn-over frequencies ranging from 790 to 850 s^{-1}. Computational investigations of the catalytic mechanism provided insights into the proposed chemical steps and detailed the energetics of electron and proton transfers.

Introduction

Nitrogen is a life-sustaining element, and the advent of the Haber–Bosch process allowed humanity to convert unreactive, atmospheric nitrogen gas into ammonia furnishing mankind with an ample supply of economical fertilizers crucial to support a burgeoning global population. However, the widespread application of these materials has precipitated disquieting perturbations within the nitrogen cycle, with the majority (>50%) of the nitrogen deployed in ammonia fertilizers reportedly escaping into the environment. Once introduced into the nitrogen cycle, this ammonia is converted to N_2O, a potent greenhouse gas, and oxyanions (*e.g.* NO_2^-, NO_3^-) that accumulate in groundwater. These byproducts, of anthropogenic origin, are documented to have negative environmental and human health effects.[1–5]

Nitrite holds a significant position in the nitrogen cycle, and revealing its electrocatalytic redox chemistry is a significant objective from both an environmental and a fundamental perspective.[6] Nature provides a model catalyst, cytochrome c nitrite reductase (CcNiR), that efficiently carries out the six electron/seven proton reduction of nitrite to ammonia and inspires chemists to discover new catalysts.[7] The search for homogeneous molecular electrocatalysts for the reduction of nitrite has been focused on Fe(III), Co(III), and Cu(II) compounds (Scheme 1). The Co(III) cyclam complex, $[Co(cyclam)Cl_2]^+$, provided an early report for electrocatalytic reduction at −1.5 V *vs.* SCE to yield hydroxylamine as the principal product with activity only observed at a mercury pool working electrode and in basic solution.[8] More recent reports of a Co(III) cyclam analogue having an unsaturated α-diimine ligand framework, **A**, electrocatalytically reduced nitrate to ammonia with 88% efficiency.[9,10] These same workers reported the Co(III) complex of a neutral tetraazamacrocylic ligand containing the redox non-innocent di(imino)pyridine moiety, **B**, transformed nitrite under electrocatalytic and acidic (−1.46 V *vs.* SCE, pH = 6.40) conditions to yield ammonium with 88% faradaic efficiency

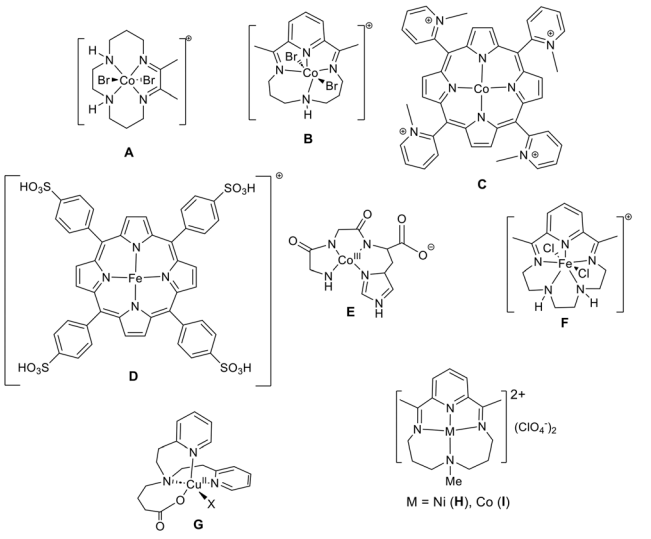

Scheme 1 Selected recent molecular electrocatalyst for nitrite reduction.

Department of Chemistry and Biomolecular Sciences, University of Ottawa, 10 Marie Curie, Ottawa, Ontario, Canada. E-mail: darrin@uottawa.ca

† Electronic supplementary information (ESI) available. CCDC 2360895. For ESI and crystallographic data in CIF or other electronic format see DOI: https://doi.org/10.1039/d4cy00715h

(FE).[11] Experimental and computational studies suggested that the ligand plays an important role in the redox chemistry.

By contrast, porphyrin complexes, [Co(2-TMPyP)][12] (2-TMPyP = tetrakis(*N*-methyl-2 pyridyl)porphine) (**C**) and [Fe(H_2O)(TPPS)]$_3$][13,14] (TPPS = (*meso*-tetrakis(*p*-sulfonatophenyl)porphyrin)), (**D**) reduced NO_2^- to NH_4^+ and NH_2OH in acidic media. Side products of N_2O and hydroxylamine appeared depending on the reaction conditions. A bio-inspired Co(III) metallotripeptide complex, **E**, showed electrocatalytic reduction of nitrite at −0.90 V *vs.* SCE using a Hg electrode in a slightly basic buffered aqueous solution (pH = 7.2). The product was ammonium with a turnover number after 5.5 hours of greater than 3500.[15]

The Fe(III) complex, **F**, displaying a macrocyclic pentadentate ligand, which also included a di(imino)pyridine group, reduced NO_2^- to NH_2OH and NH_4^+ in a buffered aqueous solution at pH 7.2 and −0.98 V *vs.* Ag/AgCl. In the absence of buffer this catalyst displayed little activity.[16]

Several Cu(II) complexes supported by tripodal N-coordinating ligands, such as **G**, have been demonstrated to reduce nitrate.[17–19] The common product from these reductions was NO and the required electrochemical potentials and Faradaic yields depend on the features of the ligand framework and solution pH.

We have a standing interest in implementing Ni(II) complexes with redox active ligands as electrocatalysts and noted a surprisingly prominent absence of Ni complexes for nitrite reduction. Some of us recently reported the selective electrocatalytic reduction of nitrite anion using redox-active macrocyclic complexes of Ni(II) (**H**) and Co(II) (**I**) as catalysts. This process yielded ammonia as the major product with excellent Faradaic efficiency and robust activity. In addition to the experimental analysis, proposed mechanistic details were elucidated through computational analysis.[20] We also recently reported the electrocatalytic hydrogen evolution activity of a simple Ni(II) diminopyridiine complex in neutral pH, aqueous saline solution.[21] We attribute a key feature of this complex to the di(imino)pyridine moiety which provides redox noninnocent functionality and postulated that these species would possess the necessary attributes for the electrocatalytic reduction of nitrogen oxyanions. We now introduce two new diiminopyridine ligated Ni(II) electrocatalysts for nitrite reduction to produce ammonium as the major product.

In addition to the nascent promise associated with the discovery of a homogenous molecular electrocatalyst for nitrite reduction, several challenges in this process are also present.[22] Nitrite reduction involves multiple electron and proton transfers and could result in several products such as NO, N_2O, NH_4^+, and NH_2OH. In addition, aqueous nitrite speciation is pH-dependent resulting in different electroactive forms.

Results and discussion

As shown in Scheme 2, two Ni compounds were synthesized through direct addition of diiminopyridine ligands to $NiBr_2$ in toluene at room temperature. The resulting orange (**1**) and yellow (**2**) powders were isolated and recrystallized from CH_2Cl_2

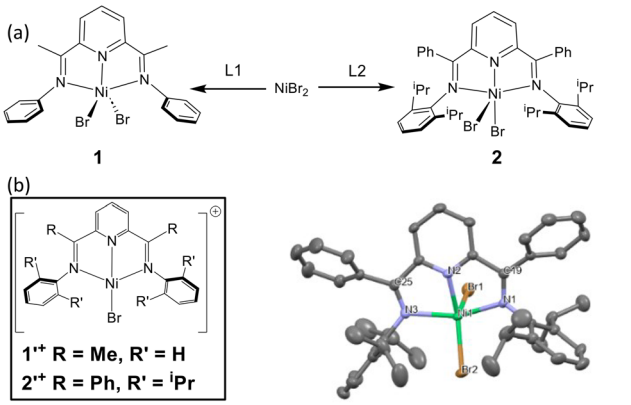

Scheme 2 (a) Synthetic method to prepare **1** and **2** and representation of the single crystal X-ray structure of **2**. (b) Autoionization product for **1** and **2** in solution.

in 88% and 68% yield respectively. The molecular structures for both compounds were confirmed through single crystal X-ray and ^{1}H NMR analysis. We previously reported the structure of compound **1** [Ni(κ^3-2,6-{PhN═CMe}$_2$(NC_5H_3))Br_2] with a trigonal bipyramidal Ni(II) center displaying a neutral planar tridentate di(imino)pyridine and two bromo ligand as shown in Scheme 2.[21] The bonding parameters were similar and consistent with other related structurally characterized species including a dichloro analogue, [Ni(κ^3-2,6-{PhN═CMe}$_2$(NC_5H_3))-Cl_2].[23] We also characterized **2** by single crystal X-ray analysis with a representation of the structure given in Scheme 2.

Compound **2** Ni{κ^3-2,6-[(^{i}Pr$_2$$C_6H_3$)N═CPh]$_2$$NC_5H_3$}$Br_2$ exhibited a mononuclear, distorted five-coordinate geometry that possessed a metal dibromide unit coordinated by the three coplanar nitrogen atoms of the di(imino)pyridine ligand. The two common limiting ideal geometries for five coordinate species are trigonal bipyramidal (tbp) and square-based pyramidal (sp) metal environments and the assignment approximate tbp or sp metal coordination geometry using a quantitative measure derived from simple calculation of structural index parameter, τ.[24–26] Application of this approach to complex **2** gives a τ parameter 0.02 indicating that the coordination geometry of **2** was best described as distorted square-based pyramidal (sp) with the basal plane defined by the nitrogen donors of the bis(imino)pyridine ligand and one of the bromides identified as Br2. The pseudo-apical position is occupied by the bromo ligand labelled Br1. The difference in coordination geometries of **1** and **2** was attributed to the structural limitations associated with the sterically demanding diisopropylphenyl substitute in **2**.

Diiminopyridinedihalonickel(II) complexes are documented to autoionize in solution to yield low spin diamagnetic, square planar d^8 species.[23,27,28] Thus solutions of **1** and **2** gave diagnostic proton ^{1}H NMR spectra indicative of a symmetrical ligand coordinated with the structure [Ni(κ^3-{PhN═CMe}$_2$(NC_5H_3))Br]$^+$ (**1**$'^+$) and structure [Ni{κ^3-2,6-[PhC═N(^{i}Pr$_2$$C_6H_3$)]$_2$$NC_5H_3$}Br]$^+$ (**2**$'^+$) and represented in inset (b) of Scheme 2. In support of this observation, during computational optimization of structures **1** and **2** (DFT, B3LYP, def2-TZVP) using the PCM

model for solvation in acetonitrile or water, spontaneous dissociation of one of the Br^- ligands to yield Ni centers with square planar geometries was observed. As a result, the dissociated bromide was removed and cationic square planar d^8 complex $\mathbf{1}'^+$ and $\mathbf{2}'^+$ (Scheme 2) were used in further computational optimizations (Fig. S1 and Table S3†).

The electrochemical characterization of **1** in acetonitrile and water has been reported.[21] For comparison, the cyclic voltammetry measurements on **2** were carried out using a 1 mM solution with 0.1 M Bu_4NPF_6 as the supporting electrolyte and with a glassy carbon (GC) working electrode, Pt counter electrode, and a Ag wire pseudo-reference electrode, which was externally referenced to the $Fc^{+/0}$ couple. The resulting cyclic voltammograms (CV) for these two species are displayed in Fig. 1. Complex **2** displayed two reversible reduction events with $E_{1/2}$ = −0.58 and −1.08 V *versus* $Fc^{+/0}$. This compares well with the two redox events observed for **1** at $E_{1/2}$ = −0.75 V and −1.15 V *versus*. $Fc^{+/0}$.[21] Both redox events displayed a linear relationship of the square root of scan speed ($v^{1/2}$) *versus* current (i) consistent with a diffusion controlled process (Fig. S2–S4†).[29]

The effect of added nitrite on the voltametric behaviour of $\mathbf{1}^+$ and $\mathbf{2}^+$ was initially probed by measuring the CVs of solutions of these species with added $NaNO_2$. A clear shift to more negative potentials was observed for the reduction events with increasing [NO_2^-] (Fig. S5 and S6†) but no signatures for catalysis, such as enhanced current, were observed during these measurements. As the NO_2^- concentration increased, the negative shift in $E_{1/2}$ potentials displayed a linear dependence on the log[NO_2^-] for both $\mathbf{1}^+$ and $\mathbf{2}^+$. These observations are consistent with nitrite association to these species which aligns with strong binding of nitrite ligation.[10,30,31]

The reduction of nitrite involves multiple proton transfer events; therefore, an aqueous buffer system was chosen to moderate any large pH changes during catalysis. Two features were considered for the selection of an appropriate buffer. The first was to choose a buffer with a conjugate base that would not strongly coordinate to the catalyst metal center. The second was to utilize a buffer that was centered at pH 7. These attributes led to the selection of the "good's buffer" derived from 4-morpholinepropanesulfonic acid (MOPS) with a pK_a of 7.20 and a pH range of 6.5–7.9, a range similar to wastewater in the environment. Moreover, MOPS has been reported as an effective buffer for this nitrite reduction catalysis.[15,16] The innocent role of MOPS in the redox chemistry of **1** was validated by observing no changes to the CV of **1** in mixed water/acetonitrile solutions the presence of MOPS buffer as shown in Fig. S7.†

The ability of complexes **1** and **2** for electrocatalytic reduction of NO_2^- reduction was then investigated by cyclic voltammetry in mixed water/acetonitrile solution employing a MOPS buffer solution at pH 6.5. As seen in Fig. 2, for both Ni complexes, the introduction of NO_2^- to the buffered solutions resulted in significant enhancement of the second reduction events with maximum current at E_{cat} = −1.23 V and E_{cat} = −1.26 V for complexes **1** and **2**, respectively. These electrochemical features were clear signatures for electrocatalytic reduction.

In order to address the possibility of background reduction at the electrode, a control experiment was carried out to establish the applied potential required to observe nitrite reduction in the absence of a catalyst. The results of cyclic voltammetry measurement of an acetonitrile/water solution in the absence of catalysts with 40 mM MOPS buffer and 50 mM $NaNO_2$ are shown in Fig. S8.† These data confirmed that applied voltages exceeding −1.7 V *vs.* $Fc^{0/+}$

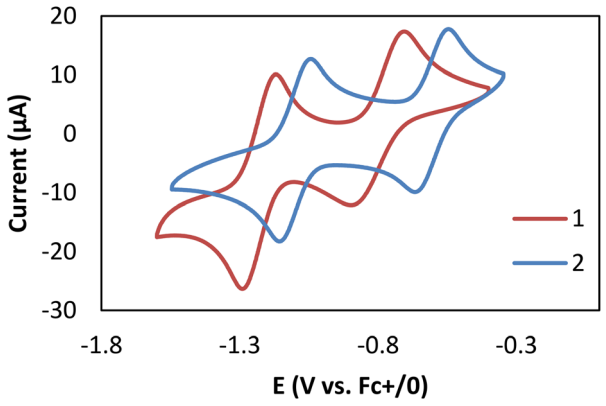

Fig. 1 Cyclic voltammogram of (1 mM) **1** (red), **2** (blue) in 50/50 CH_3CN/H_2O with 100 mM TBAHFP using a glassy carbon (GC) working electrode, Pt counter electrode and Ag pseudoreference electrode.

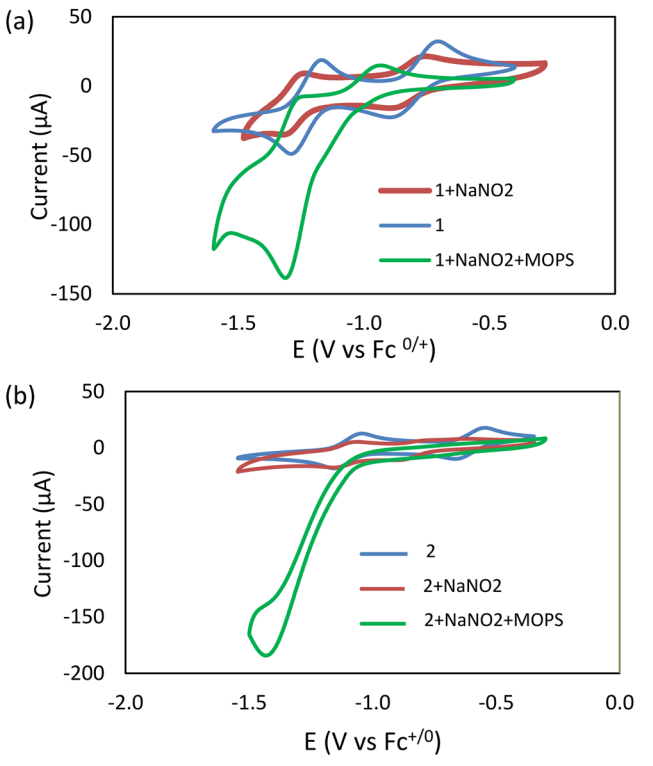

Fig. 2 CV scans of a) complex **1** and b) complex **2**. In all cases the Ni complex is 1 mM. Blue trace is for Ni complex alone. Orange is with Ni with addition of 100 mM of $NaNO_2$. Green trace is with Ni complex, 100 mM of $NaNO_2$ with addition of 40 mM MOPS. All scans in CH_3CN/H_2O (50/50) with 100 mM TBAHFP at a scan rate of 100 mV s^{-1}.

would be required to see the current enhancement associated with reduction and further demonstrated the requirement of catalysts **1** and **2** to achieve nitrite reduction at lower applied potentials.

Variation of the reduction peak current as a function of catalyst concentration was measured using complex **1**. The results are summarized in Fig. S9† and displayed a linear dependence on the concentration of [Ni(κ^3-2,6-{PhN=CMe}$_2$(NC$_5$H$_3$))Br$_2$], **1** suggesting a first order dependence on the rate of reaction.

With these reactivity characteristics established, the effect of incremental addition of $NaNO_2$ to a reaction cell containing 1 mM of Ni catalyst, 100 mM MOPS buffer (pH = 6.5), using a glassy carbon (GC) working electrode, Pt counter electrode and Ag wire pseudo-reference electrode was explored. As can be seen in Fig. S10 and S11† it was clear that after the initial addition of $NaNO_2$ to the reaction system, a significant current enhancement was observed indicative of a catalytic process. The increasing concentration of nitrite initially revealed a linear increase in the catalytic current (i_{cat}) relative to the current in the absence of substrate (i_p). Although this suggested a first-order dependence on the [NO_2^-], it is important to note that, strictly speaking, that extracting the reaction order depends on the reaction mechanism under consideration.[32] Furthermore, the catalytic current displayed a saturation behavior shifting to a pseudo-zero order rate at higher nitrite concentrations.

The ratio of the catalytic current (i_{cat}) and corresponding reductive peak current in the absence of a substrate (i_p) serves as a useful gauge to compare the activity of different catalysts.[33] The foot-of-the-wave analysis (FOWA) allows for an estimate of the reaction rate for an electrocatalytic process that does not show the limiting *S*-curve behavior.[34,35] This analysis examines the data at the earliest points in the catalytic wave, just before the catalyst reduction potential, E_{redox}. For a general multielectron catalytic system, the FOWA treatment provides eqn (1). Plotting i_{cat}/i_p *versus* $1/[1 + \exp\{(F/RT)(E - E_{redox})\}]$, where E_{redox} is the reduction potential of the catalyst, allows for extraction of the turnover frequency (TOF) for the electrocatalytic reaction of interest. The resulting curve, in the region where the applied potential approaches E_{redox}, is then fitted to a linear function and the slope of this line is given by the numerator of eqn (1). In this equation, n is the number of electrons transferred at the electrode per catalyst and n' represents the number of electrons transferred for a particular reduction. The results for this analysis are presented in Fig. S12† and yielded a TOF for **1** obtained by FOWA of 790 s^{-1}.

$$\frac{i_{cat}}{i_p} = \frac{2.24\sqrt{\frac{RT(TOF)n'}{nFv}}}{1 + \exp\left[\frac{nF}{RT}(E - E_{redox})\right]} \quad (1)$$

Similar to complex **1**, reactions of **2** with increasing [$NaNO_2$] with MOPS buffer also displayed a significant increase in current as more $NaNO_2$ was added to the system. In this case, the FOWA analysis yielded a TOF for **2** of 850 s^{-1} (Fig. S13†). These rates are quite similar to each other and substantially lower than the analogous rate obtained for complex **H** of 28 800 s^{-1}.[20] A major difference between complexes **1** and **2** and complex **H** is the presence of an additional coordinating group, the NMe moiety, which bonded to the Ni in a site *trans* to the coordinated pyridyl group. This group is absent in **1** and **2**. This suggested that the ligand may control the site of nitrite reaction on the Ni center and that reaction for **1** and **2** may occur in the ligand plane and that this reaction path may be prohibited by coordination of the NMe group in **H**.

The effect of variation of the concentration of the MOPS buffer on a catalysis was also investigated. Fig. S14† displays the result of this investigation and is consistent with the requirement of MOPS to observe catalytic behavior and with a zero-order dependence on the [MOPS]. All together these explorations support a catalytic reaction that was first order in both catalyst and nitrite with a rate law given by rate = k[cat][NO_2^-].

To determine the product identities and selectivity as well as activity and efficiency, controlled potential coulometry (CPC) experiments were explored. Measurements were carried out at −1.4 V *vs.* $Fc^{0/+}$. Typical current *vs.* time profiles are shown in Fig. S15,† which includes background current in the absence of a catalyst. The charge/time profiles in all cases displayed a steady linear increase consistent with a stable current transfer from the catalyst to the nitrite substrate.

Product analysis was carried out after 4 hours CPC at −1.4 V *vs.* $Fc^{0/+}$ in 50/50 mixed acetonitrile/water solutions using GC working and Pt counter electrodes with 100 mM tetrabutylammonium hexafluorophospate as supporting electrolyte. These solutions were buffered with MOPS at pH 6.5. Possible gas phase products N_2O or NO was scrutinized using GC and the myoglobin tests, respectively. Neither of these species was observed in these CPC experiments. To determine whether N_2 was produced, a CPC experiment was performed under argon gas and GC analysis of the reactor head space after this experiment did not show the presence of N_2. Furthermore, the reactor head space was also examined by EI mass spectroscopy and no gas phase products were observed. Spectrophotometric methods were used to determine the production of ammonium and hydroxylamine, respectively (see Fig. S16 and S17†).[36,37]

A corroborating quantitative analysis of ammonium ion was carried out using ^{14}N NMR with an internal standard for integration (see Fig. S18 and S19†).

The results for these CPC experiments are summarized in Table 1 (Table S4†) and showed that complex **1** producing 50 μmol of NH_4^+ and only 9 μmol of NH_2OH with an overall Faradaic efficiency (FE) of 54%. Under the same conditions, complex **2** generated 75 μmol NH_4^+, and no detected NH_2OH with an FE of 50%. A control experiment to measure any background product generation was also carried out under the same conditions, and neither NH_4^+ nor NH_2OH were observed. It is also noteworthy that the faradaic efficiencies of **1** and **2** while similar are lower than the >80% FE observed with the Ni complex **H**.[20] Again, these differences between the "open" bis(imino)pyridine complexes **1** and **2**

Table 1 Summary of 4 hour CPC experiments at −1.4 V *vs.* $Fc^{0/+}$ in an acetonitrile/water solution. Unless otherwise noted experiments used 1 mM catalyst (**1** or **2**) 40 mM MOPS, and 50 mM $NaNO_2$

Exp	Cat. (1 mM)	μmol NH_4^+	μmol NH_2OH	Total FE (%)
1	**1**	50	9	54
2	**2**	75	0	50
3	**No catalyst**	0	0	—
4	**1 + 100 mM NH_2OH**	197	—	73
5	**1 + N_2O**	0	0	—
6	**1 + NO**	0	0	—

with the macrocyclic bis(imino)pyridine complex **H** suggest the importance of ligand in directing the reaction path for nitrite reduction. A similar ligand steric effect may be responsible for the higher reaction rate and selectivity of **2** compared to **1**.

Interestingly, although complex **1** is documented to generate H_2 from neutral water at −1.0 V *versus* Ag/AgCl no H_2 generation was observed in the CPC measurements with nitrite anion.[21] However, in the absence of NO_2^-, electrolysis experiments with **1** at −1.4 V *vs.* $Fc^{0/+}$ over 4 hours did produce 182 μmol H_2 with 70% FE. This result suggested that the strong association of nitrite with this complex prevents competing protonation at the metal center and suppresses the hydrogen evolution process that would otherwise occur at this potential.

Several CPC experiments were also carried out in an effort to identify the reactivity of potential intermediate species in the electrocatalysis of nitrite. In particular, catalyst systems were exposed to the potential intermediate species N_2O, NO and NH_2OH and identical CPC conditions were applied. In the case of nitrous oxide, the electrochemical cell was purged with N_2O gas for 15 min prior to coulometry. No N-containing products were detected from this experiment. A similar experiment was carried out but by purging the atmosphere of the electrochemical cell with NO gas. Again, after coulometry no products were detected. However, a coulometry experiment with the same electrochemical cell configuration and a 100 mM solution of NH_2OH with 1 mM complex **1** did yield 197 μmol of NH_4^+ as the only detected product with 73% FE. The observed reduction of NH_2OH to NH_4^+ was consistent with hydroxylamine as an intermediate in the process of nitrite reduction to ammonium using catalyst **1**. Significantly, in the absence of catalyst **1** under identical experimental conditions and in the presence of NH_2OH, no ammonium was detected.

Support for the homogeneous nature of this catalysis was provided by control experiments with $\mathbf{1'}^{+}$. Linear sweep voltammetry measurements of the catalyst/substrate systems were carried out. The electrode was then carefully removed, rinsed with clean solvent, and placed in a fresh solution with substrate and no catalyst. This catalyst free system did not exhibit any electrochemical events (Fig. S20†). This suggests that $\mathbf{1'}^{+}$ had deposited on the electrode during electrolysis.

Computational analysis & proposed mechanism for NO_2^- reduction

The basis of our proposed mechanism for the electrocatalytic nitrite reduction by compounds **1** and **2** is the well-characterized mechanism for the catalytic reduction of nitrite to ammonia by cytochrome c nitrite reductase, which is based on experimental observations in conjunction with DFT computations.[38,39] To better understand, support and inform the proposed nitrite reduction reaction mechanism, density functional theory (DFT) computations were performed on these Ni complexes in water, using the polarizable continuum model (PCM) and employing the B3LYP functional. Geometry optimization and vibrational frequency calculations were performed using def2-SVP as a basis set, followed by molecular energy computations with the def2-TZVP basis set.

As shown in Scheme 3, entry to our proposed catalytic cycle begins an N-coordinated nitrite complex $\mathbf{1'(NO_2)^+}$. This species would arise from substitution of bromo ligand on $\mathbf{1'}^{+}$ by nitrite and would be consistent with our observations of the electrochemical changes observed when $NaNO_2$ is added to $\mathbf{1'}^{+}$ (Fig. S21 and S22, Table S5†). Computational optimization of this species led to a complex with a square planar Ni center displaying symmetrical bonding of the di(imino)pyridine ligand and a Ni–NO_2 bond order calculated to be 0.66 (Table S5†). The equal NO bonds in the nitrite ligand were consistent with a delocalized π bond between the N and O centers. The HOMO (MO 108) was dominated by the Ni d_{z^2} orbital and the LUMO was localized on the di(imino) pyridine ligand and exhibited π* symmetry (Fig. 3). This ligand-based LUMO provides a means for the ligand to act as an electron reservoir for electrocatalysis.[21,40,41] Furthermore, the frontier molecular orbitals that displayed significant d-orbital contribution were consistent with a square planar Ni(II) (Fig. S22†).

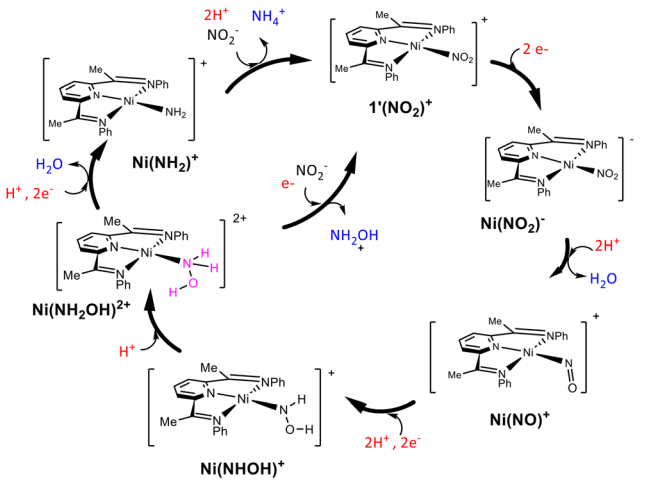

Scheme 3 A computationally supported proposed mechanism for the reduction of nitrite by complex **1**. Summary of computed thermochemistry for complexes in the proposed nitrite reduction mechanism is given in Table S11.†

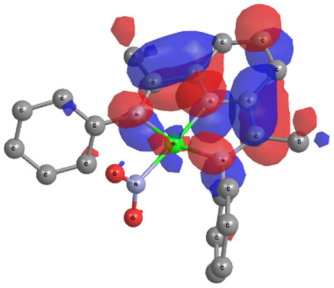

Fig. 3 The LUMO for computational optimization of $[Ni(\kappa^3\text{-}2,6\text{-}\{Ph_2PNH\}_2NC_5H_3)NO_2]^+$ ($\mathbf{1'NO_2^+}$) using the B3LYP functional, def2TZVP basis set and IEFPCM model for solvation in acetonitrile. Hydrogen atoms omitted for clarity. This orbital had major contributions from the pyridine (0.46) and the imine (0.35) fragments.

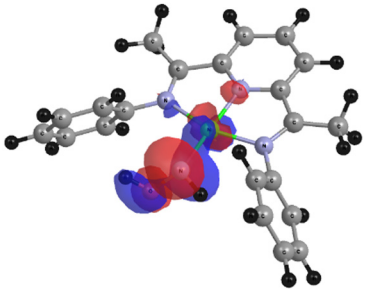

Fig. 4 The HOMO from computational optimization of $[Ni(\kappa^3\text{-}2,6\text{-}\{Ph_2PNH\}_2NC_5H_3)(N(H)OH)]^+$ ($\mathbf{Ni(NHOH)^+}$) using the B3LYP functional, def2TZVP basis set and IEFPCM model for solvation in water. This orbital had major contributions from the NH (0.50) and the OH (0.17) fragments and the Ni center (0.23).

Since catalytic activity was observed at the second reduction, the doubly reduced species, $\mathbf{Ni(NO_2)^-}$, is the first step in the cycle and this compound was examined computationally. Both singlet and triplet species were considered, and the triplet was calculated to be lower in energy by 5.3 kcal per mole. The resulting structure is shown in Fig. S23† with selected bonding parameters in Table S6.† The SOMOs for this triplet species (MO109 and 110, Fig. S24 and S25†) were dominated by Ni $d_{x^2-y^2}$ (49%) and π* delocalized over the pyridyl and imine groups of the ligand, respectively. As expected, one of the now singly occupied orbitals (MO109) is antibonding with respect the Ni center and thus, the Ni ligand bonds are lengthened relative the starting complex. The orbitals that are largely Ni d-orbital centered in nature remained essentially unchanged in comparison with the starting complex $\mathbf{1'(NO_2)^+}$.

The occupied orbital MO101 is localized on the oxygen-centers of the nitrite ligand and provided an accessible site for protonation of the $\mathbf{Ni(NO_2)^-}$ (Fig. S26†). Addition of a second proton to the coordinated nitrite resulted in spontaneous loss of water during computational optimization and formation of a nitrosyl species, $\mathbf{Ni(NO)^+}$ as shown in Fig. S27.† The calculated bonding parameters of this species given in Table S7† and the frontier orbital distribution shown in Fig. S28† suggested a bent, formally anionic nitrosyl ligand thus making assignment of the Ni as a d^8 divalent center.

Reduction and protonation of $\mathbf{Ni(NO)^+}$ would result in generation of the hydroxyamido complex $\mathbf{Ni(NHOH)^+}$. The protonation sequence is likely first at the lone electron pair on the N center represented by the HOMO of bent NO complex ($\mathbf{Ni(NO)^+}$), shown in Fig. S27,† followed by the resulting terminal oxygen site. The optimized structure of $\mathbf{Ni(NHOH)^+}$ and selected bonding parameters are given in Fig. S29 and Table S8† with the HOMO, LUMO and d-centered orbitals shown in Fig. S30.† The computed HOMO of the hydroxyamido ligand is represented in Fig. 4 and is an N-centered lone electron pair poised for protonation to yield the hydroxylamine ligated compound $\mathbf{Ni(NH_2OH)^{2+}}$.

The resulting structure and bonding of the coordinated hydroxylamine species $\mathbf{Ni(NH_2OH)^{2+}}$ (Fig. S31 and S32, Table S9†) was consistent with the proposed structure. This compound would be the source of hydroxylamine and could be an intermediate in the transformation of hydroxylamine to ammonium. An occupied MO (MO97, Fig. S33†) displayed a major density (0.56%) on the oxygen center and provided a site for protonation with release of water. Coupled with a reduction this would lead to the amido species $\mathbf{Ni(NH_2)^+}$ with the computationally optimized structure shown in Fig. S34.† The bonding parameters (Table S10†) are as would be expected for a d^8 Ni complex. The frontier orbitals for this compound are presented in Fig. S35.† Perhaps most pertinent to the mechanism is that fact that the HOMO looks like N lone pair primed for protonation, release of ammonia/ammonium and closing of the proposed cycle.

This computational mechanism has parallels to the proposed mechanism for nitrite reduction by complex **H** but does contrast in the site or reactivity at the metal center.[20] In the mechanism shown in Scheme 3, the transformation of the nitrite occurred in the ligand plane in the open site *trans* to the pyridyl group. This contrasts with the mechanism proposed using complex **H** where the nitrite reduction occurs in a site perpendicular (apical) to a square planar Ni center. These features are consistent with the suggestions that ligand coordination and sterics are significant influence on reaction rate and selectivity.

Conclusions

Increasing environmental nitrite levels are causing significant ecological and health issues, driving the search for new electrocatalysts to reduce this anion. This study introduced two new Ni(II)-based electrocatalysts for the efficient reduction of nitrite, marking a significant advancement in a field with a limited number of Ni-based examples. The results highlight structural features crucial for reactivity and selectivity, particularly indicating that steric encumbrance of the Ni center and macrocyclic coordination enhance catalyst performance.

In addition to comprehensive electrochemical characterization, a detailed computational analysis of the catalytic mechanism provided insights into the chemical steps and the energetics of electron and proton transfers.

The synergy between experimental observations and computational data suggests that the reactivity of these complexes stems from a combination of ligand redox activity and structural control. Future efforts will focus on optimizing parameters to enhance product selectivity, identifying catalysts compatible with aqueous media, and exploring the interplay between metal and ligand in bifunctional electroreduction.

Data availability

The data supporting this article have been included as part of the ESI.†

Author contributions

Somayeh Norouziyanlakvan: conceptualization, data curation, formal analysis, investigation, writing – review & editing. Jeffry Ovens: single crystal X-ray data curation and analysis. Darrin Richeson: conceptualization, funding acquisition, writing – review & editing.

Conflicts of interest

There are no conflicts to declare.

Acknowledgements

We acknowledge NSERC for funding. We also thank Professor Tom Woo for access to the Wooki cluster.

Notes and references

1 S. Matassa, D. J. Batstone, T. Hülsen, J. Schnoor and W. Verstraete, *Environ. Sci. Technol.*, 2015, **49**, 5247–5254.
2 P. M. Vitousek, J. D. Aber, R. W. Howarth, G. E. Likens, P. A. Matson, D. W. Schindler, W. H. Schlesinger and D. G. Tilman, *Ecol. Appl.*, 1997, **7**, 737–750.
3 J. Mart and J. Berbel, *Sustainability*, 2021, **13**, 5625.
4 J. G. Morrissy, M. J. Currell, S. M. Reichman, A. Surapaneni, M. Megharaj, N. D. Crosbie, D. Hirth, S. Aquilina, W. Rajendram and A. S. Ball, *Earth-Sci. Rev.*, 2021, **222**, 103816.
5 X. Zhang, B. B. Ward and D. M. Sigman, *Chem. Rev.*, 2020, **120**, 5308–5351.
6 L. B. Maia and J. J. G. Moura, *Chem. Rev.*, 2014, **114**, 5273–5357.
7 E. T. Judd, N. Stein, A. A. Pacheco and S. J. Elliott, *Biochemistry*, 2014, **53**, 5638–5646.
8 I. Taniguchi, N. Nakashima, K. Matsushita and K. Yasukouchi, *J. Electroanal. Chem. Interfacial Electrochem.*, 1987, **224**, 199–209.
9 S. Xu, D. C. Ashley, H. Y. Kwon, G. R. Ware, C. H. Chen, Y. Losovyj, X. Gao, E. Jakubikova and J. M. Smith, *Chem. Sci.*, 2018, **9**, 4950–4958.
10 S. Xu, H. Y. Kwon, D. C. Ashley, C. H. Chen, E. Jakubikova and J. M. Smith, *Inorg. Chem.*, 2019, **58**, 9443–9451.
11 S. Partovi, Z. Xiong, K. M. Kulesa and J. M. Smith, *Inorg. Chem.*, 2022, **61**, 9034–9039.
12 S. Cheng and Y. O. Su, *Inorg. Chem.*, 1994, **33**, 5847–5854.
13 M. H. Barley, K. Takeuchi, W. R. Murphy and T. J. Meyer, *J. Chem. Soc., Chem. Commun.*, 1985, 507–508.
14 M. H. Barley, K. J. Takeuchi and T. J. Meyer, *J. Am. Chem. Soc.*, 1986, **I**, 5876–5885.
15 Y. Guo, J. R. Stroka, B. Kandemir, C. E. Dickerson and K. L. Bren, *J. Am. Chem. Soc.*, 2018, **140**, 16888–16892.
16 J. R. Stroka, B. Kandemir, E. M. Matson and K. L. Bren, *ACS Catal.*, 2020, **10**, 13968–13972.
17 J. G. Woollard-Shore, J. P. Holland, M. W. Jones and J. R. Dilworth, *Dalton Trans.*, 2010, **39**, 1576–1585.
18 G. Cioncoloni, I. Roger, P. S. Wheatley, C. Wilson, R. E. Morris, S. Sproules and M. D. Symes, *ACS Catal.*, 2018, **8**, 5070–5084.
19 A. P. Hunt, A. E. Batka, M. Hosseinzadeh, J. D. Gregory, H. K. Haque, H. Ren, M. E. Meyerho and N. Lehnert, *ACS Catal.*, 2019, **9**, 7746–7758.
20 J. Ferguson, J. Brown and D. Richeson, *ChemCatChem*, 2024, **e202301168**, 1–8.
21 S. Norouziyanlakvan, J. Ferguson and D. Richeson, *Catal. Sci. Technol.*, 2022, **12**, 7494–7500.
22 S. Amanullah, P. Saha, A. Nayek, M. E. Ahmed and A. Dey, *Chem. Soc. Rev.*, 2021, **50**, 3755–3823.
23 Z. Chen, T. Wang, T. Sun, Z. Chen, T. Sheng, Y. H. Hong, Z. A. Nan, J. Zhu, Z. Y. Zhou, H. Xia and S. G. Sun, *Chin. J. Chem.*, 2018, **36**, 1161–1164.
24 E. L. Muetterties and L. J. Guggenberger, *J. Am. Chem. Soc.*, 1974, **3021**, 1748–1756.
25 A. W. Addison, T. N. Rao, J. Reedijk, J. van Rijn and G. C. Verschoor, *J. Chem. Soc., Dalton Trans.*, 1984, 1349.
26 T. Jurca, S. Ouanounou, W. Shih, T. Ong, G. P. A. Yap, I. Korobkov, S. Gorelsky and D. Richeson, *Dalton Trans.*, 2016, **45**, 14327–14334.
27 O. Luca, S. J. Konezny, E. K. Paulson, F. Habib, K. M. Luthy, M. Murugesu, R. H. Crabtree and V. S. Batista, *Dalton Trans.*, 2013, **42**, 8802.
28 O. R. Luca, S. J. Konezny, J. D. Blakemore, D. M. Colosi, S. Saha, G. W. Brudvig, V. S. Batista and R. H. Crabtree, *New J. Chem.*, 2012, **36**, 1149.
29 N. Elgrishi, K. J. Rountree, B. D. McCarthy, E. S. Rountree, T. T. Eisenhart and J. L. Dempsey, *J. Chem. Educ.*, 2018, **95**, 197–206.
30 A. J. Timmons and M. D. Symes, *Chem. Soc. Rev.*, 2015, **44**, 6708–6722.
31 W. Kaim, A. Das, J. Fiedler, S. Záliš and B. Sarkar, *Coord. Chem. Rev.*, 2020, **404**, 213114.
32 C. Costentin and J.-M. Savéant, *ChemElectroChem*, 2014, **1**, 1226–1236.
33 E. S. Rountree, B. D. Mccarthy, T. T. Eisenhart and J. L. Dempsey, *Inorg. Chem.*, 2014, **53**, 9983–10002.
34 C. Costentin, M. Robert and J.-M. Savéant, *Chem. Soc. Rev.*, 2013, **42**, 2423–2436.
35 C. Costentin, S. Drouet, M. Robert and J. M. Savéant, *J. Am. Chem. Soc.*, 2012, **134**, 11235–11242.

36 B. Hu, X. L. Tian, W. N. Shi, J. Q. Zhao, P. Wu and S. T. Mei, *Int. J. Environ. Sci. Technol.*, 2018, **15**, 323–332.
37 M. W. Weatherburn, *Anal. Chem.*, 1967, **39**, 971–974.
38 O. Einsle, A. Messerschmidt, R. Huber, P. M. H. Kroneck and F. Neese, *J. Am. Chem. Soc.*, 2002, **124**, 11737–11745.
39 W. R. Murphy, K. Takeuchi, M. H. Barley and T. J. Meyer, *Inorg. Chem.*, 1986, **25**, 1041–1053.
40 P. Berro, S. Norouziyanlakvan, G. K. Rao, B. Gabidullin and D. Richeson, *Chem. Commun.*, 2021, **57**, 9292–9295.
41 M. Ghosh, T. Weyherm and K. Wieghardt, *Dalton Trans.*, 2010, **39**, 1996–2007.